Journal of Power Sources 267 (2014) 706–713

Contents lists available at ScienceDirect

Journal of Power Sources

journal homepage: www.elsevier.com/locate/jpowsour

Improved catalytic activity of mixed platinum catalysts supported on various carbon nanomaterials

Jie Zhang [a, b, c], Shuihua Tang [a, b, *], Longyu Liao [c], Weifei Yu [c, 1], Jinshan Li [c], Frode Seland [d], Geir Martin Haarberg [d]

[a] State Key Laboratory of Oil and Gas Reservoir Geology and Exploitation, Southwest Petroleum University, Chengdu City, Sichuan 610500, PR China
[b] School of Materials and Engineering, Southwest Petroleum University, Chengdu City, Sichuan 610500, PR China
[c] Institute of Chemical Materials, China Academy of Engineering Physics, Mianyang City, Sichuan 621900, PR China
[d] Department of Materials Science and Engineering, Norwegian University of Science and Technology, Trondheim 7491, Norway

HIGHLIGHTS

- CCNTs with large specific surface area and graphitic characteristic were synthesized.
- Pt/C, Pt/CNTs, and Pt/CCNTs were mixed with different mass ratios and evaluated.
- The ECSA of Pt/C–Pt/CNTs–Pt/CCNTs (80:10:10) were calculated to be 111 $m^2\ g_{Pt}^{-1}$.
- Improved ORR activity of Pt/C–Pt/CNTs–Pt/CCNTs was obtained.

GRAPHICAL ABSTRACT

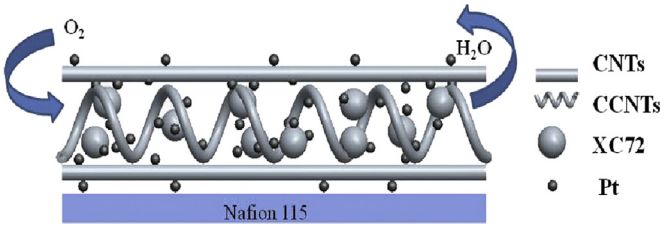

ARTICLE INFO

Article history:
Received 9 February 2014
Received in revised form
12 May 2014
Accepted 27 May 2014
Available online 5 June 2014

Keywords:
Coiled carbon nanotubes
Carbon nanotubes
Oxygen reduction reaction
Catalytic activity
Proton exchange membrane fuel cells

ABSTRACT

Electrocatalyst support affects not only catalytic activity of a catalyst, but also mass transportation and electron transfer in the catalyst layers of an electrode for proton exchange membrane fuel cells. Multi-dimensional and combined carbon materials such as Vulcan XC-72, carbon nanotubes (CNTs), and home-made coiled carbon nanotubes (CCNTs) are applied to enhance the catalyst activity and utilization. Three-dimensional CCNTs with large specific surface area and graphitic characteristic are synthesized by solid-state catalytic method. This obtained CCNTs and commercial CNTs are used as support to prepare platinum catalysts via modified ethylene glycol method, respectively. And the electrochemical surface areas (ECSAs) of the as-prepared Pt/CNTs, Pt/CCNTs and commercial Pt/C (JM) catalyst are evaluated by cyclic voltammetry. Then each two and three kinds of above catalysts mixed with different mass ratios are investigated. The ECSAs of Pt/C–Pt/CCNTs (95:5) and Pt/C–Pt/CNTs–Pt/CCNTs (80:10:10) are calculated to be 106 $m^2\ g_{Pt}^{-1}$ and 111 $m^2\ g_{Pt}^{-1}$, with respect to 70 $m^2\ g_{Pt}^{-1}$ of Pt/C (JM) catalyst. And these mixed catalysts also demonstrate improved oxygen reduction reaction activities. This is mainly attributed to the unique structure of CCNTs, which can construct a multi-dimensional network to facilitate the mass transportation and electrons/protons transfer.

© 2014 Elsevier B.V. All rights reserved.

1. Introduction

Proton exchange membrane fuel cell (PEMFC) has been regarded as an attractive and efficient power supply for portable applications due to its high efficiency, high specific energy density, zero pollution, and low operating temperature [1,2]. Pt-based

* Corresponding author. State Key Laboratory of Oil and Gas Reservoir Geology and Exploitation, Southwest Petroleum University, Chengdu City, Sichuan 610500, PR China. Tel./fax: +86 028 83032879.
E-mail addresses: shuihuatang@swpu.edu.cn, spraytang@hotmail.com (S. Tang), yuwf_1988@sohu.com (W. Yu).
[1] Tel./fax: +86 0816 2480362.

http://dx.doi.org/10.1016/j.jpowsour.2014.05.137
0378-7753/© 2014 Elsevier B.V. All rights reserved.

electrocatalysts, a kind of promising catalytic materials for widely-adapted PEMFC, provide remarkable activity for hydrogen oxidation and oxygen reduction reactions (ORR) [3]. One important goal for commercialization of PEMFC is to reduce the amount of platinum and enhance the cell performance [4]. It is generally accepted that the performance depends on the shape, size, and distribution of Pt nanoparticles. In addition, supporting material could affect not only the catalytic properties but also mass transportation and electron transfer in catalyst layers of the electrode, resulting in an enhanced catalytic activity [5]. Various carbon materials with different nanostructures and morphological characteristics have been used as support ranging from carbon black, carbon aerogels [6], carbon nanotubes, and mesoporous carbon. Carbon blacks Vulcan XC-72 has been commonly used as support for electrocatalysts in PEMFC, but the utilization of XC-72 supported catalyst is usually less than 20% due to a close packing of catalyst particles during the hot-pressing process of membrane electrode assembly (MEA) fabrication [7]. Carbon nanotubes (CNTs), with the unique morphology and physical properties including a large aspect ratio, good electrical conductivity and mechanical stability, possess the ability to carry large current densities and offer channels for fast electron/proton transfer when used for PEMFC [8–10]. The carbon nanocoils (CNCs) also realize the requirement of an ideal support for electrocatalysts, mainly due to well-defined porosity, large specific surface area of 318 $m^2\ g^{-1}$, high degree of graphitization, and good crystallinity [11].

Recently the potential application of mixed electrocatalysts has been proposed to enhance the electrochemical properties. Single-wall carbon nanotubes (SWNTs) and multi-wall carbon nanotubes (MWNTs) hybrids loaded with Pt, evaluated as the cathode catalyst layer in PEMFC, leading to an increased mass transport characteristics and cathode-specific mass activity due to a combination of the increased mass activity caused by MWNTs and the efficient proton transfer ensured by the SWNT network [12]. Shaijumon et al. [13] used [50% Pt/MWCNT + 50% Pt/C] as cathode electrocatalyst in PEMFC, and it showed the best performance of 288.9 mW cm^{-2} at voltage of 540 mV and current density of 535 mA cm^{-2} due to better dispersion of Pt nanoparticles and good accessibility of MWCNT. Graphene nanosheet (GN) also has opened up a new way to be employed as support due to its unique morphology and high electronic conductivity [14,15]. Yang et al. [16] reported that the Pd/GNS–CNTs (GN/CNTs = 5:1) exhibited the highest electrochemical active surface area (ECSA) and Pd utilization, which indicated the excellent catalytic activity and stability for formic acid electrooxidation compared to Pd/Vulcan XC-72R, Pd/GNS, or Pd/CNTs catalysts. Jafri et al. [17] pointed out that the mixture of functionalized multi-walled carbon nanotube (f-MWNT) and functionalized graphene (f-G) could also act as good catalysts supporting material for both methanol oxidation and ORR. The single cell with PtRu/(50% f-G + 50% f-MWNT) and Pt/(50% f-G + 50% f-MWNT) gave a maximum power density of 68 mW cm^{-2}.

The structures of Pt/XC-72 and Pt/XC-72–Pt/CNTs–Pt/CCNTs catalyst layer are shown schematically in Fig. 1. Spherical XC-72 carbon black is a good catalyst support but its supported Pt catalysts are easily compressed during hot-pressing process, as this will block reactants to get access to some active sites and reduce the catalyst utilization (as shown in Fig. 1a). Moreover, the electron conductivity of XC-72 is not very good. In this paper, three-dimensional coiled carbon nanotubes (CCNTs) with large specific surface area and graphitic characteristic will be applied to construct more effective mass transport channels, and one-dimensional CNTs are expected to facilitate the electron transfer (as shown in Fig. 1b). Then introduction of CCNTs and/or CNTs into the Pt/XC-72 catalysts will be designed to improve the catalytic activity and utilization of Pt/XC-72. Both two and three types of Pt/C, Pt/CNTs, and Pt/CCNTs catalysts will be mixed with different mass ratios and then investigated.

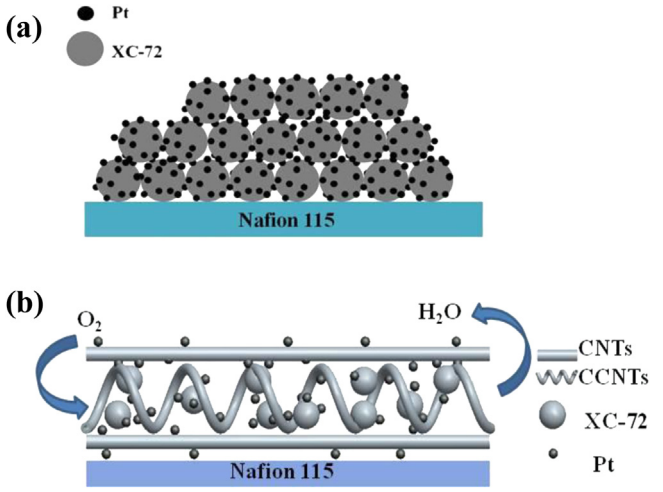

Fig. 1. The schematic structures of (a) Pt/XC-72 and (b) Pt/XC-72–Pt/CNTs–Pt/CCNTs catalyst layer.

2. Experimental

2.1. Preparation of CCNTs

CCNTs were synthesized according to the method of heat-treating mixtures of carbon precursors, silica sol, and transition-metal salts [18]. Resorcinol–formaldehyde (RF) gel was chosen as carbon precursors. Iron nitrate was used as catalyst, and silica sol (AkzoNobel chemicals Corp., particle size of SiO_2 = 4 nm; density = 1.1 g cm^{-3}) was added into the reaction mixture to achieve a high specific surface area and suitable pore size carbon material. The aqueous reaction mixture of iron nitrate/trisodium citrate/silica/resorcinol/formaldehyde with a molar ratio of 0.8:0.8:1:2:4, was cured at 85 °C for 3 h, then carbonized in an argon atmosphere at 850 °C for 3 h, followed by refluxing in 3 M NaOH to remove the silica particles and in 5 M HNO_3 to remove other residual. Eventually CCNTs were obtained after filtering, washing, and drying at 100 °C in vacuum overnight.

2.2. Preparation of electrocatalysts

Pt catalyst supported on carbon material was prepared using an improved ethylene glycol method. The required amounts of chloroplatinic acid ($H_2PtCl_6 \cdot 6H_2O$) was added to ethylene glycol (EG) under magnetic stirring, and then the pH value of the solution was adjusted with sodium hydroxide. Subsequently, the required amounts of CNTs (Chengdu Organic Chemicals Company, China) or CCNTs were added into the resulting EG solution and the obtained reaction mixture was kept at 140 °C for 3 h with an ongoing reduction process. Finally, the resulting suspension was cooled, filtered, and washed with deionized water until no chloride ions were detected, and then dried in a vacuum oven. The prepared catalysts are respectively denoted as 40 wt.% Pt/CNTs and 40 wt.% Pt/CCNTs. 40 wt.% Pt/C catalyst was obtained from Johnson Matthey Company (HiSPEC™ 4000) and referred to Pt/XC-72.

2.3. Physical characterization

Brunauer–Emmett–Teller (BET) specific surface areas were measured by nitrogen adsorption and the Barrett–Joyner–Halenda

(BJH) desorption method was applied to determine pore size distributions, using on a Quantachrome Nova Automated Gas Sorption System. The crystallinity of carbon materials and electrocatalysts was determined through X-ray diffraction (XRD) performed on a Rigaku D/MAX X-ray diffractometer equipped with Cu Kα radiation operating at 40 kV. Raman spectra were measured at room temperature with the Raman system (JY-HR800). Morphologies of carbon material and catalysts were revealed by transmission electron microscopy (TEM, Carl Zeiss SMT, Libra 200FE).

2.4. Electrochemical characterizations

Electrochemical measurements were performed using an AutoLab Potentiostat (Metrohm, Holland) with a three-electrode system at room temperature. 5 mg of the electrocatalyst was ultrasonically suspended in 1 mL of ethanol and 50 μL of Nafion® solution (5 wt.%, Du Pont) for 30 min to form a homogeneous ink. Then 25 μL of the ink was spread onto the surface of a glassy carbon electrode (GC) with a diameter of 5 mm (geometric area of 0.196 cm^2) embedded in a Teflon cylinder (Pine Instrument). A Pt wire and Ag/AgCl electrode were employed as the counter and the reference electrodes, respectively. Cyclic voltammetry (CV) was performed at room temperature between 0 and 1.4 V (vs. NHE) in 0.5 M H_2SO_4 with a scan rate of 20 mV s^{-1}. Linear sweep voltammetry (LSV) experiments were conducted in O_2-saturated 0.5 M H_2SO_4 at a scan rate of 10 mV s^{-1} and rotation rate of 1600 rpm.

3. Results and discussion

3.1. Physical characterization of carbon materials and electrocatalysts

The specific surface areas of XC-72, CNTs, and CCNTs are measured to be 215, 61, and 404 m^2 g^{-1}. The increased adsorption branch at low relative pressure and the hysteresis loop for desorption branch under the higher relative pressures of CCNTs are observed in Fig. 2a, which attributes to the hysteresis loop of type-H1 [19]. Fig. 2b shows a pore distribution of CCNTs mainly ranging from 10 to 40 nm, which indicates a typical mesoporous structure. XC-72 possesses a significant amount of mesopores [20], but CCNTs exhibit much larger mesopore volume and specific surface area than those of XC-72 and CNTs.

Fig. 3a shows the XRD patterns of XC-72, CNTs, and CCNTs. It can be seen that CCNTs indicate intensive diffraction peaks corresponding to the (002) and (100) diffraction peaks of graphite. The (002) diffraction peak of CCNTs is sharper and more intense

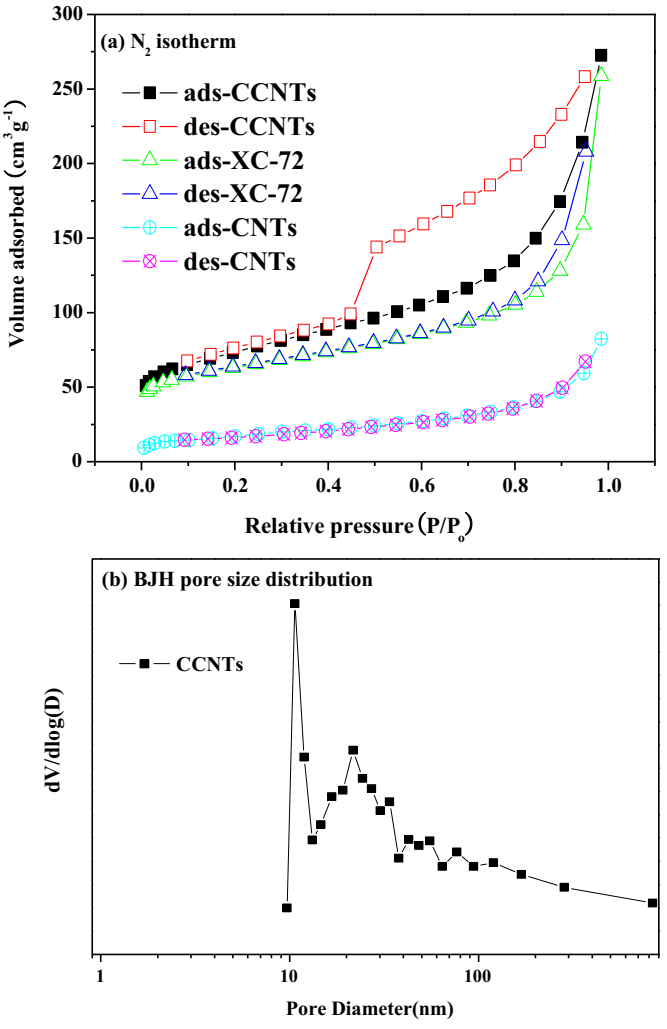

Fig. 2. (a) N_2 adsorption/desorption isotherm of carbon materials and (b) pore size distribution of CCNTs.

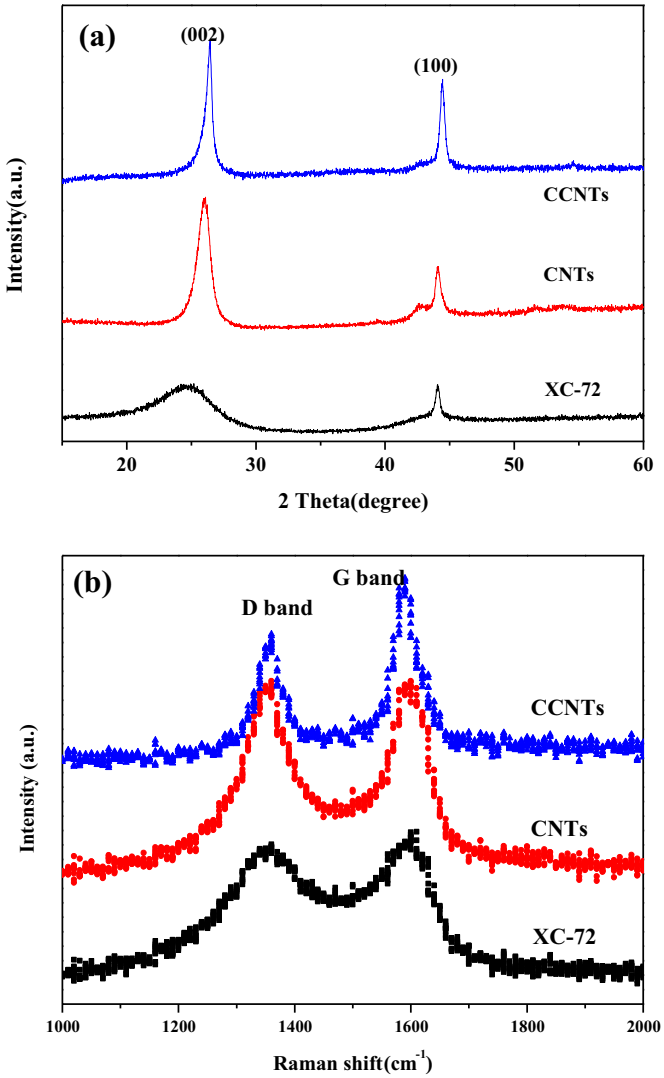

Fig. 3. (a) XRD patterns and (b) Raman spectra of various carbon materials.

than that of the XC-72 or CNTs, indicating its excellent graphitic properties. Compared to 0.3354 nm of graphite $d_{(002)}$ spacing [21], the $d_{(002)}$ of CCNTs is calculated to be 0.3387 nm using Bragg's equation based on the (002) diffraction peak, and its crystallinity is superior to that of CNTs (0.3438 nm) or amorphous XC-72 (0.3678 nm) [22]. According to Raman spectra, a G ("graphite") band peak at 1590 cm^{-1} relates to the vibration of sp^2-hybridized carbon, a D ("defect") band peak at 1350 cm^{-1} corresponds to defects, and the intensity ratio between the D and G bands (I_D/I_G) is a measure of graphitic characteristic, and the lower I_D/I_G value means a higher graphitic property [23]. As shown in Fig. 3b, CCNTs possess a lower I_D/I_G value than XC-72 and CNTs, which means it has better graphitic characteristic. This further confirms the XRD result.

The XRD patterns in Fig. 4 show a f.c.c. Pt crystalline structure of Pt/CCNTs, Pt/CNTs, and Pt/C, which is inferred from Pt (111), (200), (220), and (311) four characteristic peaks located at 39.8°, 46.2°, 67.5°, and 81.2°. The Pt (220) peak is isolated from the graphite diffraction peaks of carbon support [24], and the mean size of the Pt particles in Pt/CCNTs, Pt/CNTs, and Pt/C are calculated to be 3.7 nm, 5.8 nm, and 3.5 nm via Scherrer' formula.

As a comparison, the TEM images of XC-72 and CNTs are shown in Fig. 5a and b. XC-72 consists of spherical carbon particles with diameters of 20–50 nm. Fig. 5c displays crystalline structure of CCNTs particles consisting of the graphitic coils with a wall thickness of 5–10 nm. The observed graphitic layers are consistent with the above XRD results. Fig. 5e and f clearly reveal Pt particles distributed uniformly with a size ranging from 3 to 4 nm on XC-72 and a size distribution of 5–7 nm on CNTs. As shown in Fig. 5g, Pt particles with size ranging from 3 to 5 nm are homogeneously dispersed on CCNTs, which agrees well with the calculated results from XRD.

3.2. Electrochemical measurement of electrocatalysts

The cyclic voltammograms of Pt/CCNTs and CCNTs are shown in Fig. 6a. The ECSA of Pt can be calculated using the charge affiliated to the hydrogen underpotential adsorption or desorption [25]. The double layer charging/discharging is subtracted off the overall charge and is assumed to be similar to the charge obtained for an electrode with only CCNTs and Nafion on the GC disk electrode. A full monolayer of hydrogen is assumed to be formed on Pt catalyst surface sites corresponding to a value of $Q_H = 210\ \mu C\ cm^{-2}$. The ECSA can then be calculated using Eq. (1), where L_{Pt} is the Pt loading on the working electrode and A_g is the geometric surface area of the glassy carbon electrode.

$$\mathrm{ECSA}\left(m^2\ g_{Pt}^{-1}\right) = \left[\frac{Q_H(C)}{210\ \mu C\ cm_{Pt}^{-2}\ L_{Pt}(mg_{Pt}\ cm^{-2})\ A_g(cm^2)}\right] 10^5 \quad (1)$$

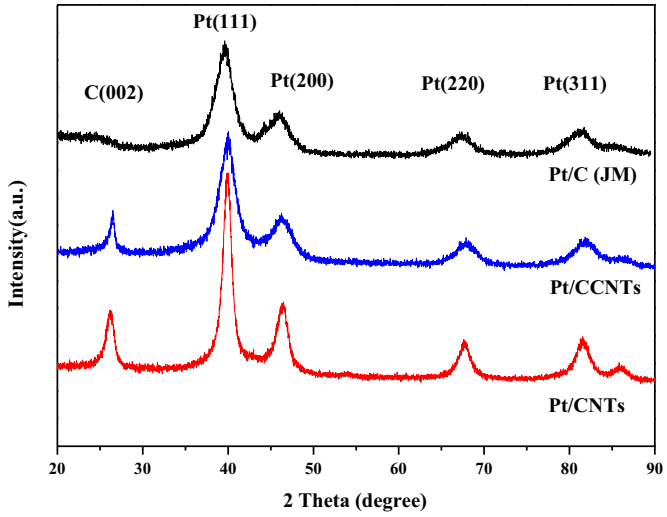

Fig. 4. XRD patterns of Pt catalysts supported on different carbon materials.

Fig. 6b shows cyclic voltammograms of Pt-electrocatalysts scanned from 0 to 1.4 V vs. NHE at a scan rate of 20 mV s^{-1} in 0.5 M H_2SO_4. According to Eq. (1), the ECSAs for Pt/C (JM), Pt/CNTs, and Pt/CCNTs are calculated to be 70, 38, and 65 $m^2\ g_{Pt}^{-1}$, respectively. The result is consistent with the mean size of Pt obtained from XRD corresponding to 3.5 nm, 5.8 nm, and 3.7 nm, respectively. Although the activities for Pt/CNTs and Pt/CCNTs are inferior compared to commercial Pt/C, addition of Pt/CNTs and/or Pt/CCNTs into the Pt/C (JM) catalyst can improve the catalytic activity of the commercial catalyst significantly, as shown by the results given below.

ECSAs for mixed catalysts of each two kinds of Pt catalysts with different mass ratios are evaluated from CV. CV curves of the mixed Pt/C and Pt/CNTs catalysts with mass ratios of 70:30, 80:20, 90:10, and 95:5 are shown in Fig. 7, and their corresponding ECSA are 74, 90, 84, and 79 $m^2\ g_{Pt}^{-1}$, respectively. The optimum ratio of Pt/C to Pt/CNTs is 80:20, its ECSA is 20 $m^2\ g_{Pt}^{-1}$ higher than that of Pt/C (JM) catalyst, even the individual Pt/CNTs shows much lower activity. It is most likely due to the fact that CNTs form a multi-dimensional network structure and establish a better conductive path [26]. However, if more than 50 wt.% of Pt/CNTs is added, a decrease in ECSA is observed. This is mainly due to the less catalytic activity contribution originating from Pt/CNTs. In order to explore the role of CNTs, CVs of Pt/C with different amounts of CNTs were recorded as shown in Fig. 8. It can be seen that Pt/C with 25 wt.% CNTs exhibits the highest ECSA of 135.5 $m^2\ g_{Pt}^{-1}$, which is obviously higher than that of Pt/C with 5 wt.% CNTs, 10 wt.% CNTs, 15 wt.% CNTs, 20 wt.% CNTs, and 30 wt.% CNTs, and their corresponding ECSAs are 77, 78, 88, 100, and 79 $m^2\ g_{Pt}^{-1}$, respectively. The result indicates that adding too large or too small amount of CNTs induces a decrease in ECSA. With the CNTs content increasing, the ECSA increases at first, which can be attributed to the formation of a porous network structure, but decreases with the excess amount of CNTs because CNTs itself does not have catalytic activity.

ECSA data calculated from Fig. 9a show that the optimum ratio of Pt/C to Pt/CCNTs is 95:5 with the ECSA value of 106 $m^2\ g_{Pt}^{-1}$. According to the BJH results, CCNTs exhibit a uniform pore size distribution (10–40 nm) and better pore volume with the increased special surface area. It proves that a very small amount of three-dimensional porous CCNTs incorporated with zero-dimensional XC-72 could contribute to a higher ECSA. Meanwhile, the mixed Pt/CCNTs and Pt/CNTs catalysts with mass ratio of 80:20 as shown in Fig. 9b show a similar ECSA value of 69 $m^2\ g_{Pt}^{-1}$ to that of Pt/C (JM) catalyst, even individual Pt/CCNTs or Pt/CNTs catalyst demonstrate poor catalytic activity.

In Fig. 10, the mixed Pt/C, Pt/CNTs, and Pt/CCNTs with mass ratio of 80:10:10 produces the highest ECSA value of 111 $m^2\ g_{Pt}^{-1}$. The three kinds of the above mentioned catalysts with mass ratio of 40:10:50 or 1:1:1 exhibit a similar Pt–H oxidation region with Pt/C (JM). However, more than 80 wt.% of Pt/C leads to an ECSA decrease, because it needs more CNTs or CCNTs to construct a multi-dimensional structure and to contact well with each other [27]. CVs of the optimized two and three kinds of mixed catalysts are shown in Fig. 11. The remarkable enhanced activity of Pt/C–Pt/CNTs–Pt/CCNTs can be explained in three aspects. Firstly, the multilayer compressed structure is avoided due to the addition of one-dimensional Pt/CNTs and three-dimensional Pt/CCNTs.

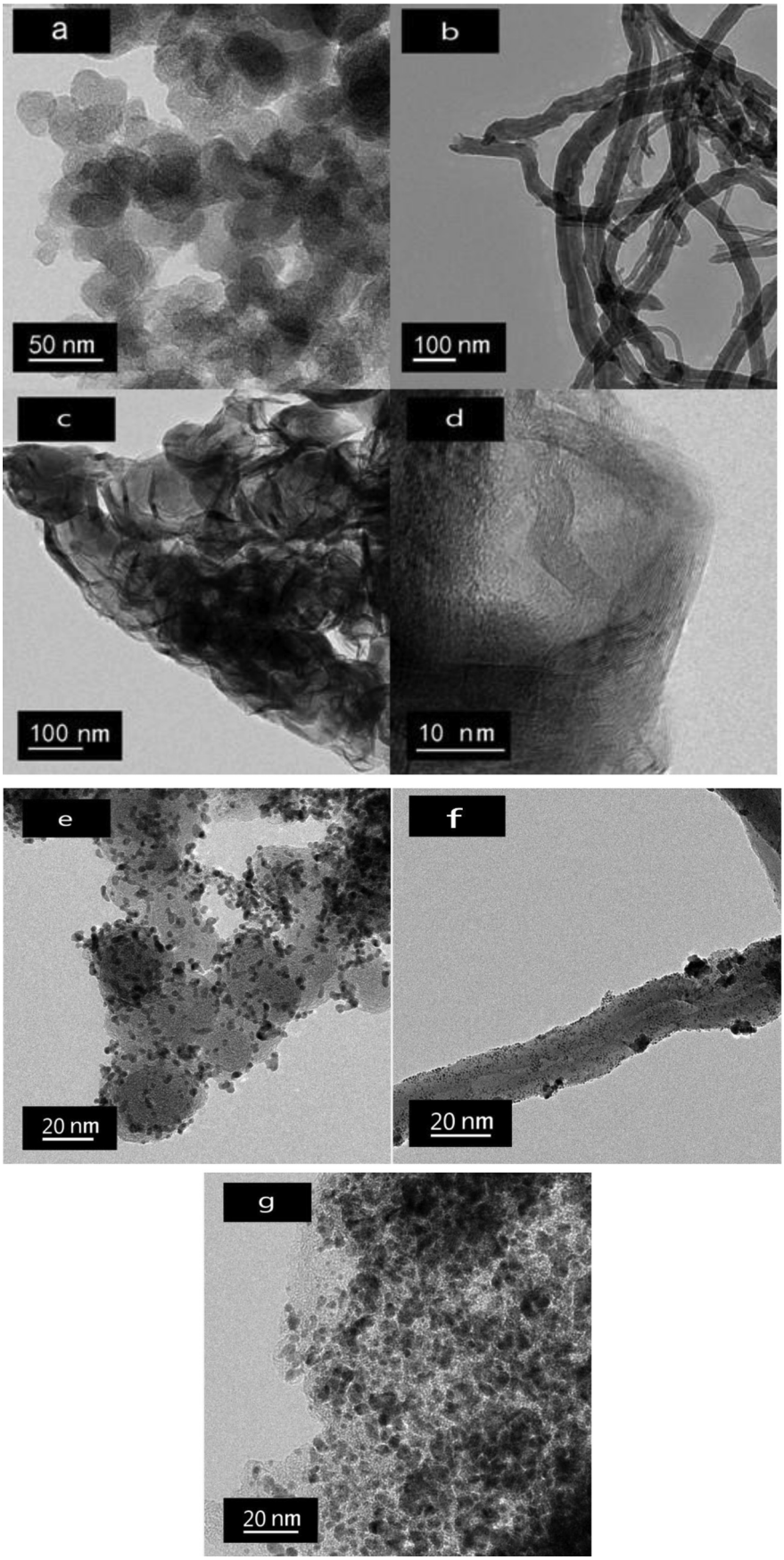

Fig. 5. TEM images of (a) XC-72, (b) CNTs, (c) and (d) CCNTs, (e) Pt/C (JM), (f) Pt/CNTs, and (g) Pt/CCNTs.

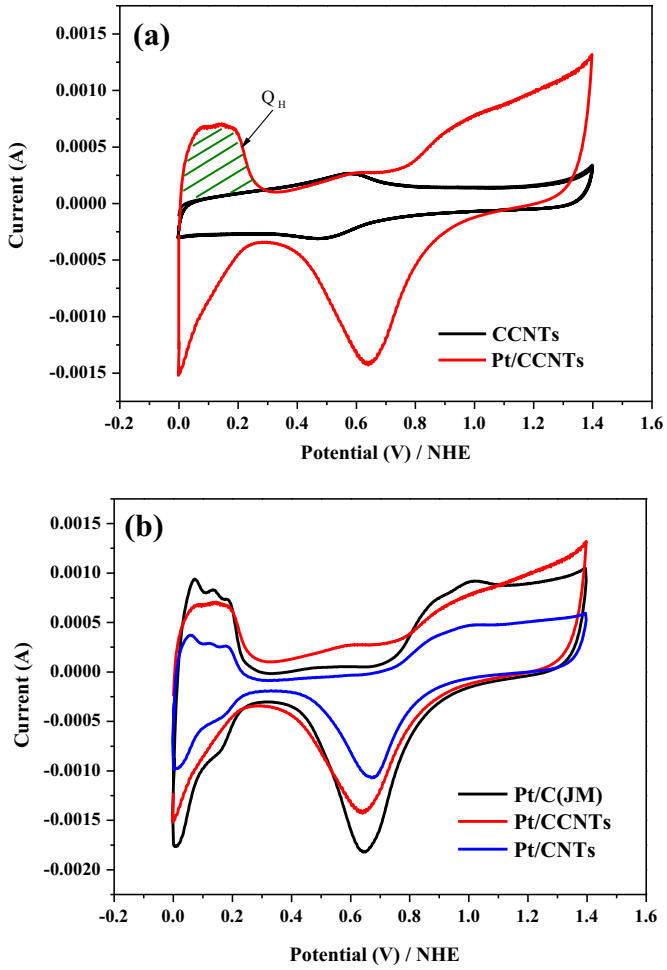

Fig. 6. Cyclic voltammograms of (a) Pt/CCNTs and CCNTs and (b) Pt/C (JM), Pt/CCNTs, and Pt/CNTs catalysts in 0.5 M H_2SO_4 with a scan rate of 20 mV s^{-1} at room temperature.

Additionally, Pt/CCNTs–Pt/CNTs work as a multi-dimensional network, promoting electrolyte through the surface of catalysts. Ultimately, we suggest that the catalytic activity contribution mainly originates from Pt/C. However, the mixed Pt/C with appropriate amounts of Pt/CNTs and/or Pt/CCNTs offered much higher ECSA values.

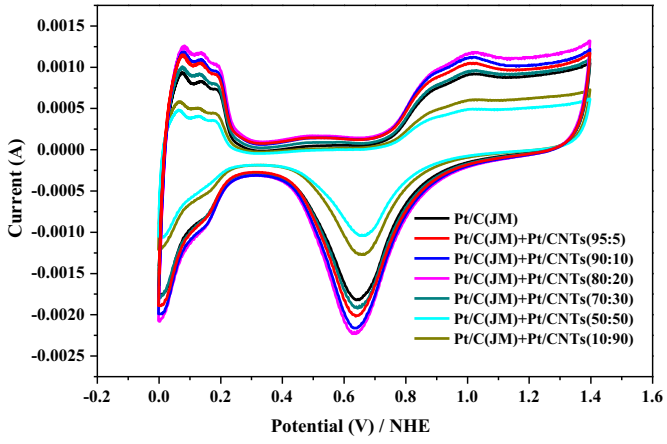

Fig. 7. Cyclic voltammograms of the mixed Pt/C and Pt/CNTs in 0.5 M H_2SO_4 with a scan rate of 20 mV s^{-1} at room temperature.

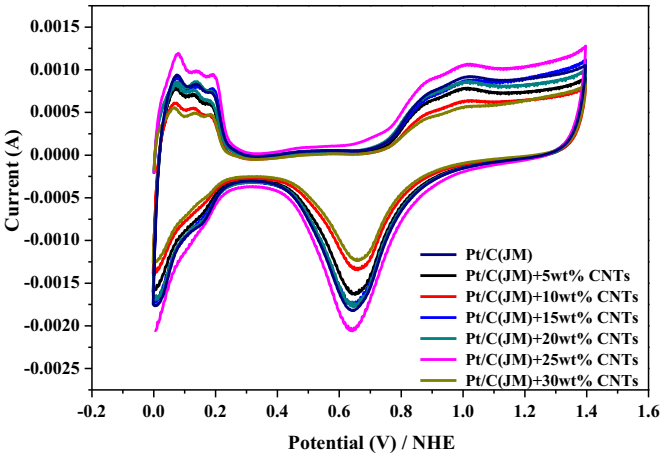

Fig. 8. Cyclic voltammograms of Pt/C with different amounts of CNTs in 0.5 M H_2SO_4 with a scan rate of 20 mV s^{-1} at room temperature.

LSV are taken to evaluate the ORR activity of catalysts. Fig. 12 shows LSV curves for the mixed two and three kinds of catalysts. The onset potential of the mixed Pt/C–Pt/CNTs–Pt/CCNTs catalysts with mass ratio of 80:10:10 is 1.1 V and similar to the commercial Pt/C catalyst. At potential of 0.7 V (vs. NHE), the current densities of the Pt/C–Pt/CNTs–Pt/CCNTs, Pt/C–Pt/CCNTs, Pt/C–Pt/CNTs, and Pt/CCNTs–Pt/CNTs are 4.7, 3.4, 3.2, and 2.2 mA cm^{-2}, compared to

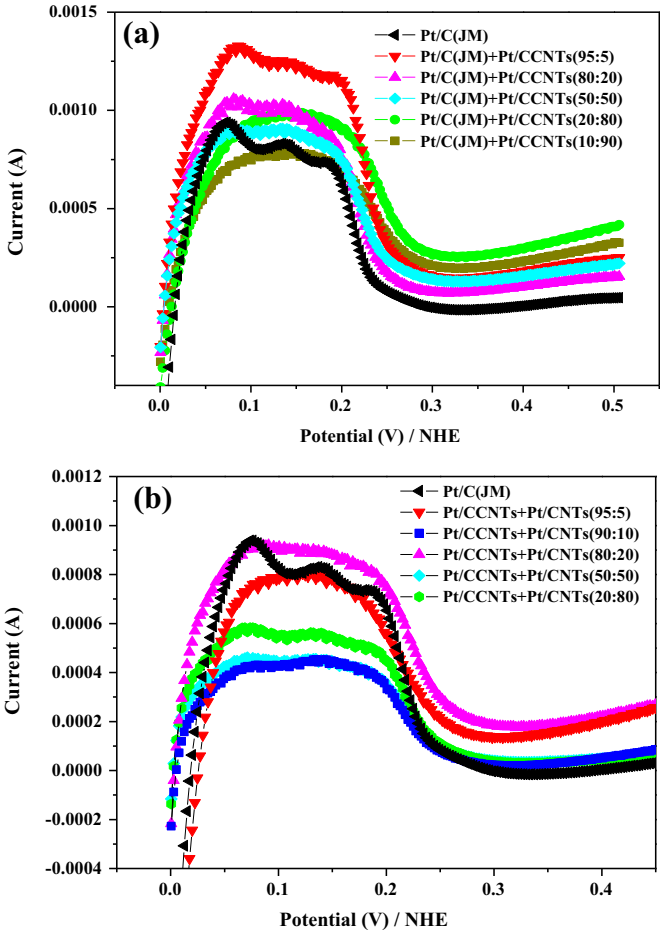

Fig. 9. Cyclic voltammograms of (a) the mixed Pt/C with Pt/CCNTs, and (b) mixed Pt/CCNTs with Pt/CNTs in 0.5 M H_2SO_4 with a scan rate of 20 mV s^{-1} at room temperature. [Only part CV curves were shown in a potential window of 0–0.5 V].

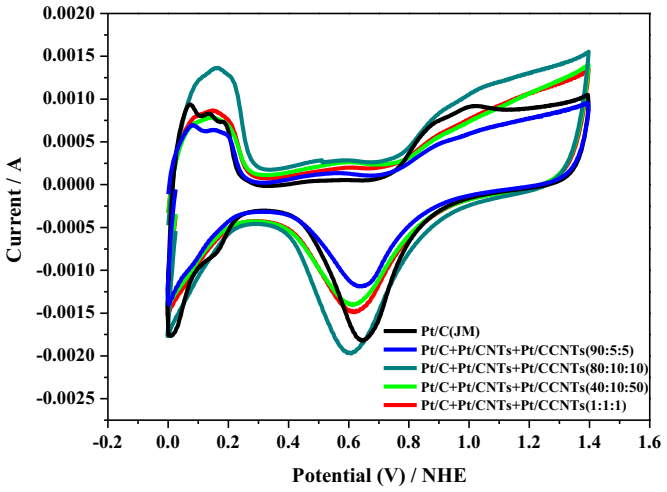

Fig. 10. Cyclic voltammograms of the mixed Pt/C with Pt/CNTs and Pt/CCNTs in 0.5 M H_2SO_4 with a scan rate of 20 mV s^{-1} at room temperature.

2.1 mA cm^{-2} of Pt/C, indicate that the mixed two or three kinds of catalysts exhibit better ORR activity. This improvement can be attributed to the more efficient mass transport in the higher current density regions, facilitating O_2 diffusion among the catalyst layers and promoting access to Pt active sites. These results are consistent with the increased ECSAs obtained from CVs.

The electrocatalytic reaction region involves solid, liquid, and gas phase transport and electron/proton transfer [28]. Based on the morphology of the three-phase region, two and three of mixed electrocatalysts with different mass ratios are employed to construct a multi-dimensional network for the sake of optimizing the electrode structure: allowing the reactant (O_2) more easily to get access to the active sites and the product (H_2O) to be quickly removed from them, thus assuring that the oxygen reduction reaction goes smoothly. The unique structure of Pt/C–Pt/CNTs–Pt/CCNTs is advantageous for the ORR pathway compared to the individual Pt/CNTs, Pt/CCNTs or Pt/C. XC-72 is a good support to disperse precious metal particles, CNTs plays the role of transferring electrons, and CCNTs are responsible for constructing preferable mass transport channels. Finally, we conceive that the mixed Pt/C with Pt/CNTs and Pt/CCNTs could be used to offer more active sites, more favorable gas-diffusion channels, and lower resistant charge-transfer paths.

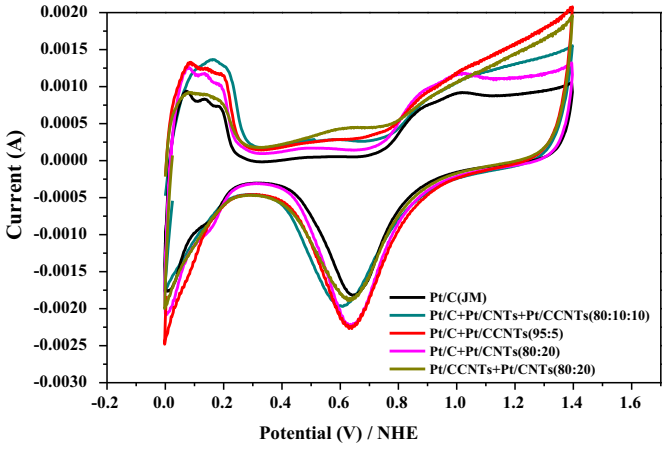

Fig. 11. Cyclic voltammograms of the optimum electrocatalysts in 0.5 M H_2SO_4 with a scan rate of 20 mV s^{-1} at room temperature.

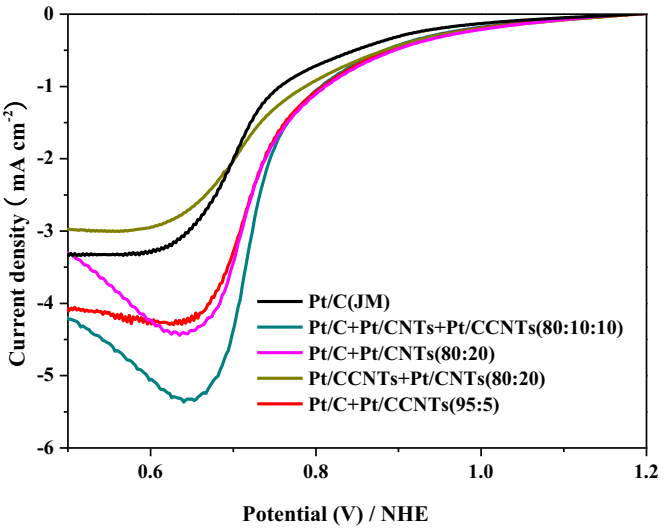

Fig. 12. LSV curves of the optimum electrocatalysts in O_2-saturated 0.5 M H_2SO_4 with a scan rate of 20 mV s^{-1} at room temperature and a rotation rate of 1600 rpm.

4. Conclusions

In this research, both two and three types of Pt/C, Pt/CNTs, and Pt/CCNTs are mixed with different mass ratios. The specific active surface areas of the mixed Pt/C and Pt/CCNTs with mass ratio of 95:5 and mixed Pt/C with Pt/CNTs and Pt/CCNTs with mass ratio of 80:10:10 are calculated to be 106 m^2 g_{Pt}^{-1} and 111 m^2 g_{Pt}^{-1} with respect to 70 m^2 g_{Pt}^{-1} for commercial Pt/C catalyst due to the unique structure of CCNTs and the enhanced conductivity of CNTs. LSV results also confirm the improved ORR activity of the mixed Pt/C with Pt/CNTs and/or Pt/CCNTs. These results indicate that two and three of the mixed platinum electrocatalysts supported on various carbon materials can significantly enhance the performance and utilization of the catalysts, and this result can be applied in practical fuel cell stacks to better the performance and reduce the amount of catalyst.

Acknowledgments

This work was supported by the Technology Project of Education Department of Sichuan Province (13ZA0193), Innovative Research Team of Southwest Petroleum University (2012XJZT002), and Scientific Research Foundation for Returned Scholars, Ministry of Education of China.

References

[1] E. Reddington, A. Sapienza, B. Gurau, R. Viswanathan, S. Sarangapani, E.S. Smotkin, T.E. Mallouk, Science 280 (1998) 1735–1737.
[2] M. Hogarth, T. Ralph, Platin. Met. Rev. 46 (2002) 146–164.
[3] T.S. Ahmadi, Z.L. Wang, T.C. Green, A. Henglein, M.A. El-Sayed, Science 272 (1996) 1924–1925.
[4] M.K. Debe, Nature 486 (2012) 43–51.
[5] S.H. Tang, G.Q. Sun, J. Qi, S.G. Sun, J.S. Guo, Q. Xin, G.M. Haarberg, Chin. J. Catal. 31 (2010) 12–17.
[6] J.S. King, A. Wittstock, J. Biener, S.O. Kucheyev, Y.M. Wang, T.F. Baumann, S.K. Giri, A.V. Hamza, M. Baeumer, S.F. Bent, Nano Lett. 8 (2008) 2405–2409.
[7] R.Z. Yang, X.P. Qiu, H.R. Zhang, J.Q. Li, W.T. Zhu, Z.X. Wang, X.J. Huang, L.Q. Chen, Carbon 43 (2005) 11–16.
[8] N. Punbusayakul, S. Talapatra, L. Ci, W. Surareungchai, P.M. Ajayan, Electrochem. Solid-State Lett. 10 (2007) 13–17.
[9] C. Soldano, S. Kar, S. Talapatra, S. Nayak, P.M. Ajayan, Nano Lett. 8 (2008) 4498–4505.
[10] S. Talapatra, S. Kar, S.K. Pal, R. Vajtai, L. Ci, P. Victor, M. Shaijumon, S. Kaur, O. Nalamasu, P.M. Ajayan, Nat. Nano 1 (2006) 112–116.
[11] T. Hyeon, S. Han, Y.E. Sung, K.W. Park, Y.W. Kim, Angew. Chem. Int. Ed. 42 (2003) 4488–4492.

[12] P. Ramesh, M.E. Itkis, J.M. Tang, R.C. Haddon, J. Phys. Chem. C 112 (2008) 9089–9094.
[13] M.M. Shaijumon, S. Ramaprabhu, N. Rajalakshmi, Appl. Phys. Lett. 88 (2006) 253105–253105-3.
[14] S. Stankovich, D.A. Dikin, G.H.B. Dommett, K.M. Kohlhaas, E.J. Zimney, E.A. Stach, R.D. Piner, S.T. Nguyen, R.S. Ruoff, Nature 442 (2006) 282–286.
[15] N. Behabtu, J.R. Lomeda, M.J. Green, A.L. Higginbotham, A. Sinitskii, D.V. Kosynkin, D. Tsentalovich, A.N.G. Parra-Vasquez, J. Schmidt, E. Kesselman, Y. Cohen, Y. Talmon, J.M. Tour, M. Pasquali, Nat. Nano 5 (2010) 406–411.
[16] S.D. Yang, C.M. Shen, X.J. Lu, H. Tong, J.J. Zhu, X.G. Zhang, H.J. Gao, Electrochim. Acta 62 (2012) 242–249.
[17] R.I. Jafri, T. Arockiados, N. Rajalakshmi, S. Ramaprabhu, J. Electrochem. Soc. 157 (2010) 874–879.
[18] J. Qi, L.H. Jiang, S.L. Wang, G.Q. Sun, Appl. Catal. B 107 (2011) 95–103.
[19] G.S. Chai, I.S. Shin, J.S. Yu, Adv. Mater. 16 (2004) 2057–2061.
[20] N.P. Subramanian, S.P. Kumaraguru, H. Colon-Mercado, H.S. Kim, B.N. Popov, T. Black, D.A. Chen, J. Power Sources 157 (2006) 56–63.
[21] M. Sevilla, C. Sanchís, T. Valdés-Solís, E. Morallón, A.B. Fuertes, J. Phys. Chem. C 111 (2007) 9749–9756.
[22] K.W. Park, Y.E. Sung, S. Han, Y. Yun, T. Hyeon, J. Phys. Chem. B 108 (2004) 939–944.
[23] M.A. Pimenta, G. Dresselhaus, M.S. Dresselhaus, L.A. Cancodo, A. Jorio, R. Sato, Phys. Chem. Chem. Phys. 9 (2007) 1276–1290.
[24] S. Mukerjee, S. Srinivasan, M.P. Soriaga, J. McRreen, J. Electrochem. Soc. 142 (1995) 1409–1422.
[25] Y. Garsany, O.A. Baturina, K.E. Swider-Lyons, S.S. Kocha, Anal. Chem. 82 (2010) 6321–6328.
[26] P. Wu, B. Li, H.D. Du, L. Gan, F.Y. Kang, Y.Q. Zeng, J. Power Sources 184 (2008) 381–384.
[27] C.F. Chi, M.C. Yang, H.S. Weng, J. Power Sources 193 (2009) 462–469.
[28] S. Litster, G. Mclean, J. Power Sources 130 (2004) 61–76.